

Superelastic Heating in Treanor-Gordiets Plasmas: A Unified Analytic Closure

Bernard Parent*

University of Arizona, Tucson, AZ 85721, USA.

In non-equilibrium plasmas where the vibrational temperature exceeds the gas temperature, conventional harmonic models underestimate superelastic electron heating rates by an order of magnitude or more. This failure stems from the artificial decoupling of energy modes, which ignores the exponential heating contributions from overpopulated high-lying states characteristic of Treanor-Gordiets distributions. We resolve this limitation by deriving a closed-form, thermodynamically consistent anharmonic gain function based on detailed balance and a second-order Dunham expansion. This formulation serves as a unified governing equation that naturally identifies the kinetic crossover between vibrational-vibrational (V-V) up-pumping and vibrational-translational (V-T) relaxation. This approach accurately predicts the Treanor minimum and recovers the accuracy of full state-to-state benchmarks at a fraction of the computational cost. The model provides a robust closure for predicting electron temperature evolution in applications ranging from hypersonic flows to plasma-assisted combustion.

ELECTRON-VIBRATIONAL (e-V) energy coupling is a cornerstone process in a diverse array of applications, including hypersonic flight, plasma-assisted combustion (PAC), laser-induced plasmas (LIP), and emerging technologies in green energy and plasma medicine. In post-shock re-entry flows, accurate T_e prediction is required for electromagnetic shielding,^{1,2} plasma antennas,³ electron transpiration cooling,^{4,5} and magnetohydrodynamic (MHD) flow control.^{6,7,8} Similarly, in PAC, accurately modeling heating pathways via electronic quenching⁹ and vibrational relaxation¹⁰ remains challenging. While detailed kinetic mechanisms exist,^{11,12} many simulations rely on phenomenological energy partition models.^{13,14} These simplified approaches often fail to capture the dynamic variation of energy transfer inherent to changing operating conditions, underscoring the need for a fully predictive formulation.

Accurate e-V modeling is equally vital for LIP,^{15,16,17} where superelastic heating becomes the governing mechanism in the inter-pulse phase once initial breakdown processes subside.^{18,19,20} Furthermore, precise treatment of vibrational-electron transfer underpins process optimization in semiconductor etching,²¹ sustainable ammonia synthesis and fuel reforming,^{22,23,24} and biomedical discharges,²⁵ where it controls vibrational up-pumping and effluent reactivity.²⁶

Despite its importance, modeling the vibrational-electron heating rate has historically been prone to error. Early phenomenological models typically scaled the heating rate using simple temperature or energy ratios.^{16,27,28} While these formulations successfully drive the system toward equilibrium ($T_e = T_v$), they lack a rigorous kinetic derivation. Conversely, more recent models founded on the principle of detailed balance^{15,17} have suffered from a subtle but critical formulation flaw: they fail to ensure the convergence of electron and vibrational temperatures at thermal equilibrium, thereby violating thermodynamic consistency.²⁹

To resolve these discrepancies, we recently introduced a thermodynamically consistent model for vibrational-electron heating.²⁹ By enforcing strict adherence to the second law of thermodynamics, this model guaranteed the correct equilibration of T_e and T_v . However, its derivation was restricted to mono-quantum transitions and assumed a Boltzmann distribution, limiting its validity to low-

temperature regimes ($T_e \lesssim 1.5$ eV). We subsequently addressed the energy limitation in a second study,³⁰ which generalized the framework to include multi-quantum overtone transitions. This extension allowed the model to be applied to high-energy discharges typical of PAC and LIP.

Nonetheless, a critical limitation remains: both prior formulations rely on the assumption of a Boltzmann distribution of vibrational states. This assumption breaks down in highly non-equilibrium regimes driven by rapid thermal energy increase—whether through strong shock heating in hypersonic flows^{31,32} or intense electron impact in plasma discharges. This deviation is particularly severe in conditions where the vibrational temperature exceeds the gas temperature ($T_v > T_g$), such as in the recombination wake of hypersonic vehicles, the inter-pulse stages of PAC, or in the non-equilibrium discharges used for chemical synthesis. In these scenarios, the electron energy is preferentially pumped into the vibrational modes while the translational mode remains cold, leading to a non-equilibrium Treanor distribution characterized by the overpopulation of high-energy states.³³ Neglecting this anharmonic distortion can lead to substantial errors in the predicted heating rates.

In this Communication, we derive a unified thermodynamic framework for electron-vibrational energy coupling. By enforcing detailed balance upon the second-order Dunham expansion, we establish an analytical governing equation for the anharmonic Treanor-Gordiets regime. This formulation resolves the limitations of conventional harmonic models, which underestimate heating, while crucially incorporating the kinetic cutoff necessary to prevent the unphysical divergence of pure Treanor scalings. The result is a robust, thermodynamically consistent description of energy transfer valid for any diatomic system driven far from equilibrium.

We derive this generalization from basic principles, ensuring the model satisfies the detailed balance principle and accounts for the anharmonicity inherent in the Treanor distribution. To extend the model to regimes where vibrational-translational non-equilibrium is significant ($T_v \neq T_g$), we relax the harmonic oscillator assumption. To ensure physical accuracy near the dissociation limit, we first establish and validate a second-order Dunham expansion for the anharmonic energy gaps.

The Dunham expansion for the energy of a vibrational level n is

*Associate Professor, bparent@arizona.edu.

typically described by the spectroscopic series:^{34,35}

$$\mathcal{E}_n = hc \left[\omega_e(n + 0.5) - \omega_e x_e(n + 0.5)^2 + \omega_e y_e(n + 0.5)^3 + \omega_e z_e(n + 0.5)^4 + \dots \right] \quad (1)$$

where h is the Planck constant, c is the speed of light, and ω_e , $\omega_e x_e$, $\omega_e y_e$, and $\omega_e z_e$ are the harmonic frequency and the consecutive anharmonic corrections. The energy gap $\Delta\mathcal{E}_{n,m}$ for a transition from level n to $n + m$ is the difference $\mathcal{E}_{n+m} - \mathcal{E}_n$.

If we truncate the series after the second anharmonic correction (neglecting terms of order $\omega_e z_e$ and higher), the energy gap is given by the exact algebraic difference:

$$\Delta\mathcal{E}_{n,m} = hc \left[m\omega_e - m\omega_e x_e(2n + m + 1) + \omega_e y_e \left((n + m + 0.5)^3 - (n + 0.5)^3 \right) \right] \quad (2)$$

In fluid models, the vibrational energy scale is anchored by the fundamental characteristic vibrational temperature $\theta_v \equiv \Delta\mathcal{E}_{0,1}/k_B$ with k_B the Boltzmann constant. To link the theoretical harmonic frequency ω_e to this macroscopic parameter, we evaluate Eq. (2) for the fundamental transition ($n = 0$, $m = 1$). Noting that the cubic term difference is $(1.5)^3 - (0.5)^3 = 3.25$, we obtain:

$$k_B\theta_v = hc\omega_e(1 - 2x_e + 3.25y_e) \quad (3)$$

Inverting this relation to express ω_e in terms of θ_v using the Taylor expansion $(1 - \epsilon)^{-1} \approx 1 + \epsilon$ (assuming small ϵ) leads to:

$$hc\omega_e \approx k_B\theta_v(1 + 2x_e - 3.25y_e) \quad (4)$$

We substitute Eq. (4) back into the general gap expression Eq. (2). Expanding the product terms and neglecting second-order cross terms (i.e., dropping $O(x_e^2)$, $O(x_e y_e)$, and $O(y_e^2)$ to maintain a linear dependence on coefficients), the terms regroup as follows:

$$\Delta\mathcal{E}_{n,m} \approx mk_B\theta_v \left[1 - x_e(2n + m - 1) + \frac{y_e}{m} \underbrace{\left((n + m + 0.5)^3 - (n + 0.5)^3 - 3.25m \right)}_{m(3n^2 + 3nm + m^2 + 3n + 1.5m - 2.5)} \right] \quad (5)$$

This yields the final unified form of the energy gap used in our model:

$$\Delta\mathcal{E}_{n,m} \approx mk_B\theta_v [1 - \delta(n, m)] \quad (6)$$

where the anharmonic defect function $\delta(n, m)$ captures the deviation from harmonicity, including both the first (x_e) and second (y_e) anharmonic corrections:

$$\delta(n, m) = x_e(2n + m - 1) - y_e(3n^2 + 3nm + m^2 + 3n + 1.5m - 2.5) \quad (7)$$

To quantify the accuracy of this formulation, we performed an error analysis for N₂ and CO. The maximum deviation of the proposed approximation occurs near the dissociation limit (approximately $n = 45$ for N₂ and $n = 80$ for CO). For a multi-quantum jump of $m = 5$, the error in the energy gap for N₂ at $n = 40$ is approximately 1.3%, confirming the model's high accuracy for nitrogen.

For CO, however, the anharmonic effects are far more pronounced. At $n = 75$ (with $m = 5$), the error of the proposed second-order formulation is approximately 7.9%. This deviation arises primarily from the algebraic linearization of cross-terms (order x_e^2) during the parameter inversion from ω_e to θ_v shown above. However, this error must be contextualized against the standard linear anharmonic approximation (neglecting y_e). In the linear case,

the model leads to a large error near dissociation, predicting a gap of only $\sim 600 \text{ cm}^{-1}$ compared to the actual $\sim 1440 \text{ cm}^{-1}$ —an error of -58%. This underprediction falsely implies that the vibrational manifold is nearly closed, which would exponentially throttle the calculated heating rate. Thus, including the second-order anharmonic term ($\omega_e y_e$) is necessary for CO to ensure physically realistic energy transfer rates near the dissociation limit. Crucially, since the population density N_n at these high vibrational levels ($n \approx 75$) is orders of magnitude lower than at the dominant energy-carrying levels ($n \approx 10$), this 7.9% local error contributes negligibly to the integrated macroscopic heating rate Q_{v-e} .

With the anharmonic energy gap established and validated, we now integrate it into the kinetic formulation. As in the harmonic derivation,³⁰ the total cooling rate Q_{e-v} is defined as the sum over all transition channels m , where m represents the change in vibrational quantum number:

$$Q_{e-v} = \sum_{m=1}^{\infty} Q_{e-v}^{(m)} \quad (8)$$

where $Q_{e-v}^{(m)}$ represents the macroscopic electron energy loss due to the specific transition channel m . The macroscopic cooling rate for channel m is obtained by summing the contributions from all vibrational levels n :

$$Q_{e-v}^{(m)} = N_e \sum_{n=0}^{\infty} N_n k_{n \rightarrow n+m} \Delta\mathcal{E}_{n,m} \quad (9)$$

where N_e is the electron number density, N_n is the population density of vibrational level n , and $k_{n \rightarrow n+m}$ is the rate coefficient for electron-impact excitation from level n to $n+m$. For the subsequent derivation, it is necessary to define the level-specific cooling flux $Q_{e-v}^{(n,m)}$, which represents the cooling contribution from the specific transition $n \rightarrow n+m$:

$$Q_{e-v}^{(n,m)} \equiv N_e N_n k_{n \rightarrow n+m} \Delta\mathcal{E}_{n,m} \quad (10)$$

The corresponding macroscopic heating rate $Q_{v-e}^{(m)}$ for the reverse superelastic processes (de-excitation from $n+m \rightarrow n$) is given by:

$$Q_{v-e}^{(n,m)} = N_e N_{n+m} k_{n+m \rightarrow n} \Delta\mathcal{E}_{n,m} \quad (11)$$

where N_{n+m} is the population of the upper state and $k_{n+m \rightarrow n}$ is the de-excitation rate coefficient. To relate these forward and reverse rates, we apply the principle of detailed balance. The rate coefficient for the reverse process is related to the forward process by the exponential of the specific anharmonic energy gap at the electron temperature T_e :

$$k_{n+m \rightarrow n} = k_{n \rightarrow n+m} \exp \left(\frac{\Delta\mathcal{E}_{n,m}}{k_B T_e} \right) \quad (12)$$

The principle of detailed balance is applied in Eq. (12) to determine the reverse rate coefficients. This step is strictly necessary to ensure the thermodynamic consistency of the formulation; utilizing independent forward and reverse rates would fail to satisfy the second law of thermodynamics at equilibrium. While this relation formally implies a Maxwellian Electron Energy Distribution Function (EEDF), this approximation is robust in the context of fluid closures. For air and nitrogen plasmas, the Maxwellian assumption is a very good approximation at moderate electron temperatures ($T_e \lesssim 2 \text{ eV}$), where the bulk distribution remains largely unaffected by inelastic losses. At higher energies, it remains a fair approximation that captures the essential physics of the energy transfer while ensuring the model converges to the correct equilibrium state.

Furthermore, we assume a Treanor distribution for the vibrationally excited states. This distribution accounts for the overpopulation of high-energy states when the vibrational temperature T_v

exceeds the translational gas temperature T_g . For a Treanor distribution, the population of a specific vibrational level n becomes:³³

$$N_n = N_0 \exp\left(-\frac{n\mathcal{E}_1}{k_B T_v} + \frac{n\mathcal{E}_1 - \mathcal{E}_n}{k_B T_g}\right) \quad (13)$$

where N_0 is the ground state population, \mathcal{E}_1 is the energy of the first vibrational level, and \mathcal{E}_n is the energy of level n . Introducing the characteristic vibrational temperature defined by $\mathcal{E}_1 \equiv k_B \theta_v$, and dividing the expression for an upper state N_{n+m} by that of a lower state N_n (where $\Delta\mathcal{E}_{n,m} = \mathcal{E}_{n+m} - \mathcal{E}_n$), yields the population ratio:

$$\frac{N_{n+m}}{N_n} = \exp\left(-\frac{m\theta_v}{T_v} + \frac{m\theta_v - \Delta\mathcal{E}_{n,m}/k_B}{T_g}\right) \quad (14)$$

Substituting the energy gap definition from Eq. (6) into Eq. (14), the population ratio simplifies compactly using the defect function $\delta(n, m)$:

$$\frac{N_{n+m}}{N_n} = \exp\left(-\frac{m\theta_v}{T_v} + \frac{m\theta_v \delta(n, m)}{T_g}\right) \quad (15)$$

We now substitute the detailed balance relation Eq. (12) and the Treanor population ratio Eq. (15) into the heating rate definition Eq. (11):

$$\begin{aligned} Q_{v-e}^{(n,m)}|_{\text{Tr}} &= N_e N_n k_{n \rightarrow n+m} \Delta\mathcal{E}_{n,m} \\ &\times \exp\left(-\frac{m\theta_v}{T_v} + \frac{m\theta_v \delta(n, m)}{T_g}\right) \exp\left(\frac{\Delta\mathcal{E}_{n,m}}{k_B T_e}\right) \end{aligned} \quad (16)$$

Next, we expand the energy gap term inside the detailed balance exponential using Eq. (6). We also recognize that the term $N_e N_n k_{n \rightarrow n+m} \Delta\mathcal{E}_{n,m}$ is exactly the definition of the cooling flux $Q_{e-v}^{(n,m)}$ given in Eq. (10). Grouping the temperature-dependent terms leads to:

$$\begin{aligned} \left.Q_{v-e}^{(n,m)}\right|_{\text{Tr}} &= \exp\left(\frac{m\theta_v}{T_e} - \frac{m\theta_v}{T_v}\right) \exp\left(-\frac{m\theta_v \delta(n, m)}{T_e} \left(1 - \frac{T_e}{T_g}\right)\right) \end{aligned} \quad (17)$$

The standard Treanor distribution physically diverges at high vibrational levels. In realistic discharges, V-T relaxation limits this growth, leading to a “Treanor-Gordiets” distribution³⁶ characterized by a plateau at high n . To model this, we consider the regime where V-T losses dominate V-V up-pumping, resulting in an approximately constant population ($N_{n+m} \approx N_n$). We assume a simplified flat plateau characteristic of strong V-T domination. While exact Gordiets distributions may exhibit a slope, this approximation captures the essential suppression of the Treanor divergence without the cost of solving the full master equation. Substituting $N_{n+m} \approx N_n$ and the detailed balance relation Eq. (12) into the heating rate definition Eq. (11), and utilizing the cooling flux definition from Eq. (10), we obtain the heating flux for the plateau regime:

$$Q_{v-e}^{(n,m)}|_{\text{Pl}} = Q_{e-v}^{(n,m)} \exp\left(\frac{\Delta\mathcal{E}_{n,m}}{k_B T_e}\right) \quad (18)$$

Substituting the anharmonic energy gap approximation from Eq. (6) into the exponential, and multiplying and dividing by $\exp(m\theta_v/T_v)$, yields:

$$\left.Q_{v-e}^{(n,m)}\right|_{\text{Pl}} = \exp\left(\frac{m\theta_v}{T_e} - \frac{m\theta_v}{T_v}\right) \exp\left(\frac{m\theta_v}{T_v} - \frac{m\theta_v \delta(n, m)}{T_e}\right) \quad (19)$$

To close the formulation, we must identify the physically consistent heating rate Q_{v-e} . We observe that the ratio of the heating flux to the cooling flux is intrinsically tied to the population distribution. Dividing the definition of the superelastic heating flux (Eq. 11) by the

cooling flux (Eq. 10) and applying the principle of detailed balance (Eq. 12) yields a direct proportionality:

$$\frac{Q_{v-e}^{(n,m)}}{Q_{e-v}^{(n,m)}} = \frac{N_{n+m}}{N_n} \exp\left(\frac{\Delta\mathcal{E}_{n,m}}{k_B T_e}\right) \quad (20)$$

Since the exponential term depends solely on the electron temperature T_e , the flux ratio serves as a direct kinetic proxy for the local population ratio N_{n+m}/N_n . Consequently, the physical competition that governs the population density—between V-V up-pumping and V-T relaxation—must similarly constrain this flux ratio.

Physically, the actual population distribution follows the lower envelope of these two limiting regimes. At low vibrational levels, V-V exchange dominates, forcing a thermodynamic decay ($N_{n+m} < N_n$); here, the Treanor ratio is less than unity, correctly predicting the population drop, whereas the Plateau approximation would unphysically predict a constant density near N_0 . Conversely, at high vibrational levels, anharmonic pumping drives the Treanor prediction to diverge ($N_{n+m} > N_n$); in this regime, rapid V-T relaxation imposes a “ceiling,” enforcing the Plateau limit.

Thus, the physically valid solution is always the one corresponding to the smallest population ratio. Because the heating-to-cooling ratio scales linearly with this population ratio, we introduce the generalized correction factor $\Phi_{\text{anh}}^{(n,m)}$ to enforce this minimum constraint within the heating formulation:

$$\frac{Q_{v-e}^{(n,m)}}{Q_{e-v}^{(n,m)}} = \Phi_{\text{anh}}^{(n,m)} \exp\left(\frac{m\theta_v}{T_e} - \frac{m\theta_v}{T_v}\right) \quad (21)$$

where the correction factor is given by the minimum of the two kinetic limits:

$$\Phi_{\text{anh}}^{(n,m)} = \min\left(\exp\left[-\frac{m\theta_v \delta(n, m)}{T_e} \left(1 - \frac{T_e}{T_g}\right)\right], \exp\left[\frac{m\theta_v}{T_v} - \frac{m\theta_v \delta(n, m)}{T_e}\right]\right) \quad (22)$$

The expression inside the minimum function shares a common dependence on the electron temperature. Factoring out the term $-\frac{m\theta_v \delta(n, m)}{T_e}$ allows us to separate the kinetic detailed balance limit from the population reservoir limits:

$$\Phi_{\text{anh}}^{(n,m)} = \exp\left[-\frac{m\theta_v \delta(n, m)}{T_e}\right] \min\left(\exp\left[\frac{m\theta_v \delta(n, m)}{T_g}\right], \exp\left[\frac{m\theta_v}{T_v}\right]\right) \quad (23)$$

Since the exponential function is monotonic, the minimum operation can be moved inside the exponent. This yields the compact, physically transparent form:

$$\Phi_{\text{anh}}^{(n,m)} = \exp\left(m\theta_v \left[\min\left(\frac{\delta(n, m)}{T_g}, \frac{1}{T_v}\right) - \frac{\delta(n, m)}{T_e}\right]\right) \quad (24)$$

Isolating the channel-specific heating term $Q_{v-e}^{(n,m)}$ in Eq. (21) and summing over all channels m and all vibrational levels n , the total heating rate becomes:

$$Q_{v-e} = \sum_{n=0}^{\infty} \sum_{m=1}^{\infty} Q_{e-v}^{(n,m)} \Phi_{\text{anh}}^{(n,m)} \exp\left(\frac{m\theta_v}{T_e} - \frac{m\theta_v}{T_v}\right) \quad (25)$$

This formulation generalizes the thermodynamically consistent model to Treanor-Gordiets distributions. By utilizing the minimum function, the model inherently captures the competition between the limiting kinetic mechanisms—Treanor up-pumping at low levels and V-T relaxation at high levels—yielding a unified description of the energy transfer. This guarantees a robust closure for predicting electron temperature evolution across the full range of non-equilibrium conditions.

To verify the physical rigor of this formulation, we examine if the model correctly identifies the transition from the Treanor regime to the V-T dominated plateau. Inspection of Eq. (24) reveals that the magnitude of $\Phi_{\text{anh}}^{(n,m)}$ is determined by the minimum of the Treanor and plateau constraints within the exponential argument. Consequently, the switch between these kinetic regimes occurs naturally when these competing terms coincide:

$$\frac{\delta(n, m)}{T_g} = \frac{1}{T_v} \quad (26)$$

To determine the location of this transition, we apply the linear anharmonic approximation to the defect function, $\delta(n, m) \approx x_e(2n - 1)$ (neglecting second-order y_e terms and assuming the continuous limit $m \rightarrow 0$ for the population distribution). Solving for the vibrational level n yields the critical crossover point:

$$n^* \approx \frac{T_g}{2x_e T_v} + \frac{1}{2} \quad (27)$$

This result recovers the standard definition of the Treanor minimum n^* , the vibrational level where V-V up-pumping balances V-T relaxation. Consequently, the “Min” function in Eq. (24) serves as a rigorous analytical identification of the physical transition from the Treanor regime to the plateau regime intrinsic to the population distribution.

A second test we can perform to verify the physical accuracy of this formulation is to demonstrate that it satisfies strict thermodynamic consistency at thermal equilibrium. We consider the limit of complete thermal equilibrium where the electron temperature, vibrational temperature, and translational gas temperature are identical:

$$T_e = T_v = T_g = T \quad (28)$$

Substituting these equalities into the total heating rate expression in Eq. (25), we examine the two temperature-dependent components individually. First, the harmonic scaling term (the first exponential) vanishes because $T_e = T_v = T$:

$$\exp\left(\frac{m\theta_v}{T_e} - \frac{m\theta_v}{T_v}\right) \Big|_T = \exp(0) = 1 \quad (29)$$

Second, we examine the anharmonic correction factor $\Phi_{\text{anh}}^{(n,m)}$ defined in Eq. (24). Under the condition $T_e = T_g = T_v = T$, the expression becomes:

$$\Phi_{\text{anh}}^{(n,m)} \Big|_T = \exp\left(\frac{m\theta_v}{T} [\min(\delta(n, m), 1) - \delta(n, m)]\right) \quad (30)$$

To evaluate the minimum function, we recall the definition of the anharmonic energy gap $\Delta\mathcal{E}_{n,m} \approx m k_B \theta_v [1 - \delta(n, m)]$. For all bound vibrational states, the energy gap must be positive ($\Delta\mathcal{E}_{n,m} > 0$), which implies that the defect function satisfies $\delta(n, m) < 1$. Consequently, the minimum function selects the anharmonic defect:

$$\min(\delta(n, m), 1) = \delta(n, m) \quad (31)$$

Substituting this back into the exponent, the term $-\delta(n, m)$ from the detailed balance limit cancels perfectly with the term $+\delta(n, m)$ from the Treanor population limit:

$$\Phi_{\text{anh}}^{(n,m)} \Big|_T = \exp\left(\frac{m\theta_v}{T} [\delta(n, m) - \delta(n, m)]\right) = \exp(0) = 1 \quad (32)$$

Substituting these results back into Eq. (25), the expression for the total heating rate simplifies to the sum of the level-specific cooling fluxes:

$$Q_{v-e}|_T = \sum_{m=1}^{\infty} \sum_{n=0}^{\infty} [Q_{e-v}^{(n,m)} \cdot 1 \cdot 1] = \sum_{m=1}^{\infty} \sum_{n=0}^{\infty} Q_{e-v}^{(n,m)} \quad (33)$$

By definition, the term $Q_{e-v}^{(n,m)}$ is the cooling flux for a specific transition (Eq. 10). Summing these fluxes over all levels n yields the macroscopic cooling rate per channel $Q_{e-v}^{(m)}$ (Eq. 9), and summing over all channels m recovers the total cooling rate Q_{e-v} (Eq. 8). Thus, we recover the strict equality:

$$Q_{v-e} = Q_{e-v} \quad \text{when } T_v = T_e = T_g \quad (34)$$

This proves that the generalized model is thermodynamically consistent. It ensures zero net energy transfer when the electrons are fully thermalized with both the vibrational and translational modes of the gas.

While consistency holds at strict *thermal equilibrium* ($T_e = T_v = T_g$), it is critical to distinguish this state from the *two-temperature quasi-equilibrium* where the electron temperature equilibrates only with the vibrational temperature ($T_e = T_v$), while the gas temperature remains distinct ($T_v \neq T_g$). This latter regime gives rise to the classic Treanor distribution. Under these conditions, the harmonic scaling term in Eq. (25) reduces to unity. However, because $T_e \neq T_g$, the anharmonic correction factor $\Phi_{\text{anh}}^{(n,m)}$ defined in Eq. (24) does not vanish. Instead, in the physically relevant regime where vibrational pumping occurs ($T_v > T_g$), the correction factor assumes a value greater than unity ($\Phi_{\text{anh}}^{(n,m)} > 1$). This behavior is verified by inspecting the exponent in Eq. (24). Under the condition $T_e = T_v > T_g$, the subtraction term reduces to $\delta(n, m)/T_v$. Since $T_v > T_g$ implies $\delta(n, m)/T_g > \delta(n, m)/T_v$, and the bound state condition $\delta(n, m) < 1$ implies $1/T_v > \delta(n, m)/T_v$, the expression inside the square brackets remains positive regardless of which limit the minimum function selects. Consequently, the net exponent is positive, rendering the correction factor greater than unity ($\Phi_{\text{anh}}^{(n,m)} > 1$).

This result is physically consistent. In a Treanor-Gordiets distribution, the vibrational population densities deviate substantially from the Boltzmann distribution defined by the single parameter T_v . High-energy vibrational states are overpopulated relative to the harmonic prediction. Since the free electrons exchange energy with this distorted, anharmonic population manifold, the net heat flux does not vanish simply because T_e matches the low-level fundamental temperature T_v . Therefore, the electron temperature does not strictly equilibrate with T_v in the Treanor limit. Instead, the persistent non-zero net flux pumps the electron energy, driving T_e toward a generalized equilibrium value that exceeds the fundamental vibrational temperature ($T_e > T_v$). The final electron temperature is determined by the competition with cooling mechanisms. While electron-translational (e-T) relaxation provides a baseline anchor to the gas temperature, it is often insufficient to counteract anharmonic pumping. In these cases, the electron temperature rises significantly above T_v until it is ultimately clamped by inelastic electronic excitation and ionization thresholds. Thus, in the absence of strong elastic coupling, the electron fluid is sustained at a quasi-steady temperature defined by these high-energy loss barriers rather than by thermal equilibration with the gas.

Having established the theoretical consistency of the model, we now turn to its numerical implementation and validation. The implementation of the generalized heating model relies on the determination of the vibrational temperature, T_v . In multi-temperature fluid models, the specific vibrational energy e_v is typically the transported conserved variable. Conversely, in state-to-state (StS) models, the population densities of explicitly tracked vibrational levels are evolved. While StS approaches theoretically allow for the direct summation of heating rates over all transitions, ensuring thermodynamic consistency (where $Q_{e-v} = Q_{v-e}$ at thermal equilibrium) requires accounting for the full spectrum of hot-band processes. In practice, rate coefficients for many of these high-lying transitions are unavailable, and their omission leads to unavoidable violations of the second law of thermodynamics, as demonstrated in Ref. 30.

The macroscopic model derived in Eq. (25) overcomes this limitation by enforcing thermodynamic consistency analytically. Consequently, even in StS frameworks, it is preferable to compute heating using the present model. This necessitates mapping the instantaneous energy distribution to an equivalent T_v .

Regardless of whether an StS or energy transport framework is employed, T_v is determined as follows. The specific vibrational energy e_v is defined as the population-weighted average of the energy levels:

$$e_v = \left(\sum_{n=0}^{n_{\max}} N_n \mathcal{E}_n \right) \left(\sum_{n=0}^{n_{\max}} N_n \right)^{-1} \quad (35)$$

where N_n is the population density of vibrational level n , and $\mathcal{E}_n = nk_B\theta_v[1-\delta(0,n)]$ is the energy of level n relative to the ground state, calculated using the defect function $\delta(n,m)$ defined in Eq. (7). The upper limit of the summation, n_{\max} , corresponds to the highest bound vibrational level before molecular dissociation. This is determined by finding the root n of the equation $\mathcal{E}_n = D_0$, where D_0 is the dissociation energy of the molecule (or the vertex of the anharmonic parabola if D_0 exceeds the Morse potential maximum). For N_2 , solving for $D_0 \approx 9.76$ eV yields $n_{\max} \approx 45$. Following the same procedure for other common diatomics, $n_{\max} \approx 38$ for NO and $n_{\max} \approx 80$ for CO.

To ensure consistency with the heating rate derivation, the population distribution must reflect the Treanor-Gordiets profile utilized in Eq. (24). We approximate this distribution by following the Treanor curve up to the transition level n^* derived in Eq. (27), which corresponds to the minimum of the Treanor distribution. For levels $n > n^*$, we assume a constant plateau dominated by V-T relaxation. The explicit form for the population in the Treanor regime ($n \leq n^*$) is obtained directly from Eq. (15) by setting the lower state to the ground level (0) and the transition jump to $m = n$. This yields the population of level n relative to the ground state N_0 :

$$N_n = \begin{cases} N_0 \exp\left(-\frac{n\theta_v}{T_v} + \frac{n\theta_v\delta(0,n)}{T_g}\right) & \text{if } n \leq n^* \\ N_{n^*} & \text{if } n > n^* \end{cases} \quad (36)$$

where N_0 is the ground state population density. Substituting this distribution into Eq. (35), the factor N_0 cancels out, and the unknown vibrational temperature T_v corresponding to a specific energy e_v is found by determining the root of the residual function $R(T_v)$:

$$R(T_v) = e_v - \left(\sum_{n=0}^{n_{\max}} N_n(T_v) \mathcal{E}_n \right) \left(\sum_{n=0}^{n_{\max}} N_n(T_v) \right)^{-1} \quad (37)$$

We employ the Newton-Raphson method to solve $R(T_v) = 0$. A robust initial guess T_v^0 is provided by the analytical harmonic inversion:

$$T_v^0 = \frac{\theta_v}{\ln(1 + k_B\theta_v/e_v)} \quad (38)$$

Given the monotonic nature of the energy-temperature relationship below the dissociation limit, this iterative procedure typically converges within a few iterations.

To validate the closed-form heating rate derived in Eq. (25), we perform a direct numerical comparison against a full state-to-state (StS) summation in 0D. This provides a test of the model's ability to resolve the enhanced heating flux driven by the pumping of high-energy populations in the Treanor limit, without the confounding factors of a full 3D simulation.

We consider a representative N_2 plasma characterized by a fixed electron temperature $T_e = 2.0$ eV and a fixed gas temperature $T_g = 300$ K. The vibrational temperature T_v varies into highly non-equilibrium states. For each value of T_v , the population distribution N_n is constructed explicitly using the Treanor-Gordiets formulation

described in Eq. (36), with $n_{\max} = 45$. To ensure physically realistic heating magnitudes typical of discharge plasmas, we specify an electron number density of $N_e = 10^{19}$ m⁻³ and a total nitrogen number density of $N_{\text{tot}} \approx 10^{25}$ m⁻³, corresponding to a pressure of approximately 0.4 atm.

To ensure validation remains independent of species-specific resonances, we employ a canonical synthetic scaling law for the forward excitation rates:

$$k_{n \rightarrow n+m} = A(n+1) \exp(-0.5m) \quad (39)$$

where $A = 3.0 \times 10^{-16}$ m³/s. The term $(n+1)$ captures standard harmonic bond stretching, while $\exp(-0.5m)$ accounts for the probability decay of multi-quantum jumps. This formulation isolates the thermodynamic impact of the population distribution from the stochastic variations of specific cross-section datasets.

Three distinct methods were used to calculate the total superelectronic electron heating rate Q_{v-e} . First, the exact StS benchmark heating rate was calculated by a brute-force summation where the heating contribution of every individual transition channel was determined via the principle of detailed balance applied locally to that specific reaction. This approach sums the energy released from each de-excitation event ($n+m \rightarrow n$) using the exact population densities N_{n+m} and the anharmonic energy gaps. Second, the standard harmonic model heating rate was computed using the scaling which assumes a Boltzmann distribution and ignores anharmonicity. This corresponds to Eq. (25) with $\Phi_{\text{anh}} = 1$. Third, the generalized model heating rate was computed using the proposed closed-form analytic expression in Eq. (25), incorporating the anharmonic correction factor Φ_{anh} defined in Eq. (24).

The results are presented in Fig. 1. At low vibrational temperatures where $T_v \approx T_g$, the distribution remains Boltzmann-like, and all three models converge to the same result. However, as T_v increases beyond 3000 K, the non-equilibrium Treanor effect causes a substantial overpopulation of high-energy vibrational states. Consequently, the harmonic approximation physically diverges from the actual kinetic state. It remains blind to the high-energy anharmonic reservoir populated by up-pumping, effectively decoupling the electron fluid from the dominant energy storage mode. This results in an order-of-magnitude collapse in the predicted coupling strength (dashed blue line). In contrast, the generalized model captures the anharmonic physics inherent in the Φ_{anh} factor and reproduces the exact StS summation with negligible error. This agree-

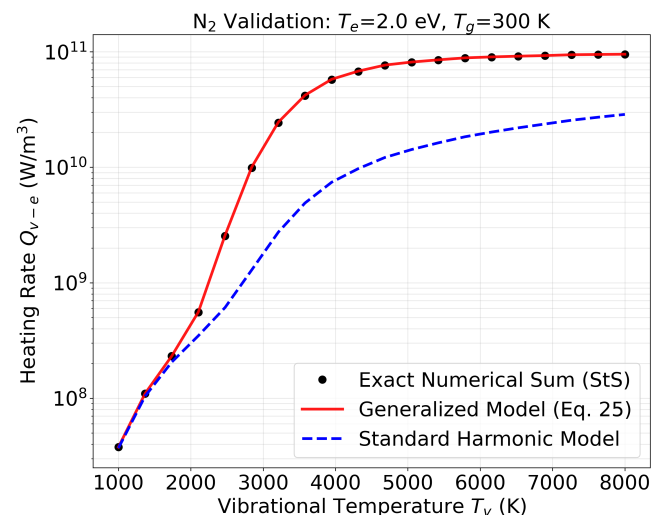


Fig. 1: Comparison of vibrational-electron heating rates for N_2 at $T_e = 2$ eV and $T_g = 1000$ K.

ment confirms that Φ_{anh} functions not merely as a correction factor, but as the requisite entropic bridge connecting the linear Boltzmann regime to the highly non-equilibrium Treanor manifold. It restores thermodynamic consistency without the computational intractability of state-to-state kinetics.

I. Data Availability

The data that support the findings of this study are available from the author upon reasonable request.

References

- [1] Musal, H., "On the theory of the radar-plasma absorption effect," *GM Defense Res. Laboratories, Santa Barbara, CA*, 1963.
- [2] Gregoire, D., Santoru, J., Schumacher, R., et al., "Electromagnetic-wave propagation in unmagnetized plasmas," *AD-A250710*, 1992.
- [3] Magarotto, M., Sadeghikia, F., Schenato, L., Rocco, D., Santagiustina, M., Galtarossa, A., Horestani, A. K., and Capobianco, A.-D., "Plasma antennas: A comprehensive review," *IEEE Access*, 2024. <https://doi.org/10.1109/ACCESS.2024.3411142>.
- [4] Hanquist, K. M., Hara, K., and Boyd, I. D., "Detailed modeling of electron emission for transpiration cooling of hypersonic vehicles," *Journal of Applied Physics*, Vol. 121, No. 5, 2017. <https://doi.org/10.1063/1.4974961>.
- [5] Parent, B., Hanquist, K., Thoguluva Ranjendran, P., and Liza, M., "Effect of Cesium Seeding on Plasma Density in Hypersonic Boundary Layers," 2021, AIAA Paper 2021-1251. <https://doi.org/10.2514/6.2021-1251>.
- [6] Moses, R. W., Cheatwood, F. M., Johnston, C. O., Macheret, S. O., Parent, B., Little, J., Williams, R., Green, J. S., Austin, M., and Aldrin, A., "New MHD Lift Concept for More Efficient Missions to Mars and Neptune," *AIAA SCITECH 2022 Forum*, 2022, AIAA Paper 2022-0934. <https://doi.org/10.2514/6.2022-0934>.
- [7] Parent, B., Thoguluva Rajendran, P., Macheret, S. O., Little, J., Moses, R. W., Johnston, C. O., and Cheatwood, F. M., "Effect of Plasma Sheaths on Earth-Entry Magnetohydrodynamics," *Journal of thermophysics and heat transfer*, Vol. 37, No. 4, 2023, pp. 845–857. <https://doi.org/10.2514/1.T6784>.
- [8] Parent, B., Rodriguez Fuentes, F. M., and LaFoley, S., "Electrodeless Magnetohydrodynamic Local Force Generator for Aerocapture," *AIAA Journal*, Vol. 63, No. 8, 2025, pp. 3035–3047. <https://doi.org/10.2514/1.J064125>.
- [9] Bak, M. S., Kim, W., and Cappelli, M. A., "On the quenching of excited electronic states of molecular nitrogen in nanosecond pulsed discharges in atmospheric pressure air," *Applied Physics Letters*, Vol. 98, No. 1, 2011, pp. 011502. <https://doi.org/10.1063/1.3535986>.
- [10] Adamovich, I. V., Macheret, S. O., Rich, J. W., and Treanor, C. E., "Vibrational Energy Transfer Rates Using a Forced Harmonic Oscillator Model," *Journal of Thermophysics and Heat Transfer*, Vol. 12, No. 1, 1998, pp. 57–65. <https://doi.org/10.2514/2.6302>.
- [11] Adamovich, I. V., Li, T., and Lempert, W. R., "Kinetic mechanism of molecular energy transfer and chemical reactions in low-temperature air-fuel plasmas," *Philosophical Transactions of the Royal Society A: Mathematical, Physical and Engineering Sciences*, Vol. 373, 2015, pp. 20140336. <https://doi.org/10.1098/rsta.2014.0336>.
- [12] Chen, B.-S., Garner, A. L., and Bane, S. P. M., "Numerical analysis of a nanosecond repetitively pulsed plasma-assisted counterflow diffusion flame," *Journal of Applied Physics*, Vol. 133, No. 203302, 2023. <https://doi.org/10.1063/5.0147305>.
- [13] Castela, M., Fiorina, B., Coussement, A., Gicquel, O., Darabiha, N., and Laux, C. O., "Modelling the impact of non-equilibrium discharges on reactive mixtures for simulations of plasma-assisted ignition in turbulent flows," *Combustion and Flame*, Vol. 166, 2016, pp. 133–147. <https://doi.org/10.1016/j.combustflame.2016.01.009>.
- [14] Dijoud, R. J., Laws, N., and Guerra-Garcia, C., "Mapping the performance envelope and energy pathways of plasma-assisted ignition across combustion environments," *Combustion and Flame*, Vol. 271, 2025, pp. 113793. <https://doi.org/10.1016/j.combustflame.2024.113793>.
- [15] Peters, C. J., Shneider, M. N., and Miles, R. B., "Kinetics model of femtosecond laser ionization in nitrogen and comparison to experiment," *Journal of applied physics*, Vol. 125, No. 24, 2019. <https://doi.org/10.1063/1.5098306>.
- [16] Shneider, M., Zheltikov, A., and Miles, R., "Long-lived laser-induced microwave plasma guides in the atmosphere: Self-consistent plasma-dynamic analysis and numerical simulations," *Journal of Applied Physics*, Vol. 108, No. 3, 2010. <https://doi.org/10.1063/1.3457150>.
- [17] Pokharel, S. and Tropina, A., "Self-consistent model and numerical approach for laser-induced non-equilibrium plasma," *Journal of Applied Physics*, Vol. 134, No. 22, 2023. <https://doi.org/10.1063/5.0175177>.
- [18] Radziemski, L. J. and Cremers, D. A., *Laser-Induced Plasmas and Applications*, Marcel Dekker Inc., New York, NY, 1989. <https://doi.org/10.1201/9780585250917>.
- [19] Alberti, A., Munafò, A., Koll, M., Nishihara, M., Pantano, C., Freund, J. B., Elliott, G. S., and Panesi, M., "Laser-induced non-equilibrium plasma kernel dynamics," *Journal of Physics D: Applied Physics*, Vol. 53, No. 2, 2019, pp. 025201. <https://doi.org/10.1088/1361-6463/ab44ce>.
- [20] Munafò, A., Alberti, A., Pantano, C., Freund, J. B., and Panesi, M., "A computational model for nano-second pulse laser-plasma interactions," *Journal of Computational Physics*, Vol. 406, 2020, pp. 109190. <https://doi.org/10.1016/j.jcp.2019.109190>.
- [21] Kushner, M. J. and Zhang, D., "An electron impact cross section set for CHF_3 ," *Journal of Applied Physics*, Vol. 88, No. 6, 2000, pp. 3231–3234. <https://doi.org/10.1063/1.1289076>.
- [22] Arakoni, R. A., Bhoj, A. N., and Kushner, M. J., "H₂ generation in Ar/NH₃ microdischarges," *Journal of Physics D: Applied Physics*, Vol. 40, No. 8, 2007, pp. 2476–2490. <https://doi.org/10.1088/0022-3727/40/8/010>.
- [23] Jiang, J., Richards, C., Adamovich, I., and Bruggeman, P. J., "Molecular beam mass spectrometry measurements of vibrationally excited N₂ in the effluent of an atmospheric plasma jet: a comparison with a state-to-state kinetic model," *Plasma Sources Science and Technology*, Vol. 31, No. 10, oct 2022, pp. 10LT03. <https://doi.org/10.1088/1361-6595/ac954c>.
- [24] Miyake, A., Shirai, N., and Sasaki, K., "Contribution of vibrationally excited molecular nitrogen to ammonia synthesis using an atmospheric-pressure plasma jet," *Journal of Applied Physics*, Vol. 135, No. 21, 2024, pp. 213301. <https://doi.org/10.1063/5.0208655>.
- [25] Bruggeman, P. J., Kushner, M. J., Locke, B. R., Gardeniers, J. G. E., Graham, W. G., Graves, D. B., Hofman-Caris, R. C. H. M., Maric, D., Reid, J. P., Ceriani, E., Fernandez Rivas, D., Foster, J. E., Garrick, S. C., Gorbanev, Y., Hamaguchi, S., Iza, F., Jablonowski, H., Klimova, E., Kolb, J., Krcma, F., Lukes, P., Machala, Z., Marić, I., Mariotti, D., Mededovic Thagard, S., Minakata, D., Neyts, E. C., Pawlat, J., Petrovic, Z. L., Pflieger, R., Reuter, S., Schram, D. C., Schröter, S., Shiraiwa, M., Tarabová, B., Tsai, P. A., Verlet, J. R. R., von Woedtke, T., Wilson, K. R., Yasui, K., and Zvereva, G., "Plasma-liquid interactions: a review and roadmap," *Plasma Sources Science and Technology*, Vol. 25, No. 5, 2016, pp. 053002. <https://doi.org/10.1088/0963-0252/25/5/053002>.

[26] Davies, H. L., Guerra, V., van der Woude, M., Gans, T., O'Connell, D., and Gibson, A. R., "Vibrational kinetics in repetitively pulsed atmospheric pressure nitrogen discharges: average-power-dependent switching behaviour," *Plasma Sources Science and Technology*, Vol. 32, No. 1, 2023, pp. 014003. <https://doi.org/10.1088/1361-6595/aca914>.

[27] Kim, M., Gülbah, A., and Boyd, I. D., "Modeling of electron energy phenomena in hypersonic flows," *Journal of thermophysics and heat transfer*, Vol. 26, No. 2, 2012, pp. 244–257. <https://doi.org/10.2514/1.T3716>.

[28] Farbar, E., Boyd, I., and Martin, A., "Numerical Prediction of Hypersonic Flowfields Including Effects of Electron Translational Nonequilibrium," *Journal of Thermophysics and Heat Transfer*, Vol. 27, No. 4, 2013, pp. 593. <https://doi.org/10.2514/1.T3963>.

[29] Rodriguez Fuentes, F. M. and Parent, B., "Vibrational-Electron Heating in Plasma Flows: A Thermodynamically Consistent Model," *Physics of Fluids*, Vol. 37, No. 096141, 2025. <https://doi.org/10.1063/5.0285170>.

[30] Parent, B. and Rodriguez Fuentes, F. M., "Thermodynamically consistent vibrational-electron heating: Generalized model for multi-quantum transitions," *Physics of Fluids*, Vol. 38, No. 1, jan 2026, pp. 011705. <https://doi.org/10.1063/5.0314083>.

[31] Singh, N. and Schwartzenruber, T. E., "Nonequilibrium internal energy distributions during dissociation," *Proceedings of the National Academy of Sciences*, Vol. 115, No. 1, 2018, pp. 47–52. <https://doi.org/10.1073/pnas.1713840115>.

[32] Parsons, N. S., Zhu, T., Levin, D. A., and van Duin, A. C. T., "Modeling of molecular nitrogen collisions and dissociation processes for direct simulation Monte Carlo," *The Journal of Chemical Physics*, Vol. 141, No. 23, 2014, pp. 234307. <https://doi.org/10.1063/1.4903782>.

[33] Treanor, C. E., Rich, J. W., and Rehm, R. G., "Vibrational relaxation of anharmonic oscillators with exchange-dominated collisions," *The Journal of Chemical Physics*, Vol. 48, No. 4, 1968, pp. 1798–1807. <https://doi.org/10.1063/1.1668914>.

[34] Dunham, J. L., "The Energy Levels of a Rotating Vibrator," *Physical Review*, Vol. 41, No. 6, 1932, pp. 721–731. <https://doi.org/10.1103/PhysRev.41.721>.

[35] Herzberg, G., *Molecular Spectra and Molecular Structure. I. Spectra of Diatomic Molecules*, D. Van Nostrand Company, Princeton, NJ, 2nd ed., 1950.

[36] Gordiets, B. F., Osipov, A. I., and Shelepin, L. A., "Kinetic processes in gases and molecular lasers," *Moscow Izdatel Nauka*, 1980.